Stress fluctuations in sheared Stokesian suspensions

J. Dasan and T. R. Ramamohan*
Computational Materials Science, Unit-I, Regional Research Laboratory (CSIR), Thiruvananthapuram 695 019, India

Anugrah Singh and Prabhu R. Nott†
Department of Chemical Engineering, Indian Institute of Science, Bangalore 560 012, India

We report an analysis, using the tools of nonlinear dynamics and chaos theory, of the fluctuations in the stress determined from simulations of shear flow of Stokesian suspensions. The simulations are for shear between plane parallel walls of a suspension of rigid identical spheres in a Newtonian fluid, over a range of particle concentration. By analyzing the time series of the stress, we find that the dynamics underlying these fluctuations is deterministic, low-dimensional, and chaotic. We use the dynamic and metric invariants of the underlying dynamics as a means of characterizing suspension behavior. The dimension of the chaotic attractor increases with particle concentration, indicating the increasing influence of multiple-body interactions on the rheology of the suspension with rise in particle concentration. We use our analysis to make accurate predictions of the short-term evolution of a stress component from its preceding time series, and predict the evolution of one component of the stress using the time series of another. We comment on the physical origin of the chaotic stress fluctuations, and on the implications of our results on the relation between the microstructure and the stress.

I. INTRODUCTION

Rheological properties of suspensions are examples of spatial averages over a large number of elements, which are individually chaotically varying (here the suspended particles exhibit chaotic motion), showing a variety of interesting behavior. The bulk stress in a suspension of small particles in a fluid depends on many factors, of which particle concentration, the Stokes number (which characterizes the importance of particle inertia in comparison with viscous forces), colloidal and Brownian forces, and flow type are important. The dynamic interaction of these factors determines the suspension microstructure, from which the macroscopic rheological properties follow. Particulate suspensions are, of course, encountered frequently in a variety of industrial processes, and understanding their rheology can provide significant commercial benefit. Moreover, suspensions are useful models of spatially extended chaotic systems, which can be analyzed both theoretically and experimentally, and their rheological properties represent easily measurable spatial averages over the positions of all the particles.

It is well known that the stress in a particulate suspension exhibits strong fluctuations about a well-defined average. The fluctuations increase in magnitude with the particle concentration and are easily measurable in experiments, but only the temporal average is usually reported. Stress fluctuations in suspension flows have been observed in the simulations of pressure-driven flows and simple shear flow [1,2]. However, we are unaware of any study that has attempted to analyze these fluctuations.

It is now widely recognized that the fluctuations in the properties of nonlinear systems convey useful information on their dynamics. The utilization of the tools of nonlinear dynamics has led to the possibility of uncovering information about the underlying dynamics of a system whose output is in the form of a fluctuating time series [3–5]. Our broad objectives in this work are to see whether these tools [6,7], when applied to fluctuations in the bulk stress of Stokesian suspensions, can capture information about their underlying dynamics, and hence lead to a way of characterizing their behavior by proper estimates of the dynamical and topological (geometrical) invariants of the fluctuating time series, such as dimension estimates, Lyapunov exponents, principal eigenvalues, etc. Some of the possible advantages of studying fluctuations in rheological properties using the tools of nonlinear dynamics and chaos theory are (i) the identification of the existence of a low-dimensional attractor leading to the possibility of intelligent chaos control; (ii) accurate short-range predictions of fluctuations; (iii) predicting fluctuations in properties that are difficult to measure (such as the shear stress) from those that are easy to measure (such as the normal stress on a boundary); and (iv) using the invariant measures of the dynamics in design and scale-up of equipment.

From a fundamental viewpoint, we expect that an analysis of the stress fluctuations will provide useful information on the microstructure, or arrangement of particles during shear. For Stokesian suspensions, the stress is simply a product of the fluid viscosity, the shear rate, and a function of the microstructure. Hence, fluctuations in the stress reflect directly fluctuations in the microstructure. For dilute suspensions, hydrodynamic interactions may be assumed to be pairwise, and the stress is therefore determined by the pair distribution function. Batchelor and Green [8] determined analytically the steady-state pair distribution function for pure straining flow assuming only hydrodynamic interactions between particles, and thereby computed the $O(\phi^2)$ correction to the

*Electronic address: trr432@yahoo.com
†Electronic address: prnott@chemeng.iisc.ernet.in

suspension viscosity. More recently, Brady and Morris [9] determined the pair distribution function for shear flow for a weakly Brownian suspension with a repulsive interparticle force in addition to the hydrodynamics. They found that the repulsive interaction breaks the fore-aft symmetry of the pair distribution function, and therefore leads to finite normal stress differences in the suspension. Both these studies considered unbounded flows for which there is a time-independent steady state in the microstructure for dilute suspensions. In the concluding section of this paper, we comment on the origin of fluctuations in the microstructure and the implications of our results on the relation between stress and microstructure.

In this paper, we report results obtained from a detailed analysis of the fluctuations of the stresses of a non-Brownian suspension of spheres in simple shear flow, for a range of particle concentration and Couette gap. We present numerical evidence for the existence of a low-dimensional chaotic attractor in the rheological properties. This indicates that the fluctuations of the rheology arise from low-dimensional deterministic dynamics. We use this information to predict successive fluctuations of the stress from the preceding fluctuations. We also use this to perform a cross prediction of the time series of one stress component from the time series of another, and indicate the potential of this approach. We find that the invariant measures such as the correlation dimension, Lyapunov exponent, etc., that characterize the fluctuations change with rise in concentration, suggesting changes in the microstructure with increasing concentration. The correlation dimension for the normal and shear stresses is approximately the same for a constant area fraction of particles and we also observed that the values of the maximum Lyapunov exponents for different stress components are roughly the same for a fixed particle concentration. From our results we draw interesting conclusions on the relation between the microstructure and rheology of the suspension.

II. RHEOLOGY OF SUSPENSIONS

Determination of the macroscopic properties of suspensions from the fluid mechanics around the particles originated from Einstein's celebrated work [10], in which he considered the dilute limit where particle interactions are absent. Batchelor and Green [8] derived the $O(\phi^2)$ contribution to the viscosity, ϕ being the particle volume fraction, resulting from binary particle interactions. Determining the bulk stress analytically at higher concentrations has not been possible, as it requires computation of many-body hydrodynamic interactions as well as knowledge of the statistics of the position distribution of particles. A large number of studies have examined the shear viscosity of suspensions either by experimentation or numerical simulations, with the implicit assumption that their behavior is Newtonian. Recently, Brady and Morris [9] argued that the presence of a nonhydrodynamic interaction force, however small, results in non-Newtonian effects such as normal stress differences. Though it is not clear that nonhydrodynamic forces are necessary, normal stress differences have been measured experimentally in non-Brownian suspensions by Gadala-Maria [11], Zarraga *et al.* [12], and Singh and Nott [13], and in numerical simulations by Singh and Nott [2].

The studies cited above do not address the issue of fluctuations in the stress, but attempt to determine the time and space averaged bulk stress in the suspension for a prescribed flow field (Singh and Nott [2] have commented on the fluctuations, but have not analyzed them). From a microstructural viewpoint, fluctuations in the stress are caused by temporal changes in the microstructure, which in turn arise from two sources: (i) The chaotic motion of individual particles in the suspension, and (ii) fluctuations in the spatially averaged microstructure due to a coupling between its evolution and the flow. The former exists even in molecular systems, but its characteristic time scale is so small that it is unimportant in the hydrodynamic sense. In suspension flows, the only time scale is that imposed by the shear rate, and therefore the effects of the two mechanisms listed above are indistinguishable. The important point is that these fluctuations have not been studied, and it is our belief that examining them through the conceptual lens of nonlinear dynamics would be of significant benefit.

III. IMPLICATIONS OF CHAOS THEORY

Prior to the development of methods of analysis for nonlinear systems, any irregularly varying data were assumed to either be not amenable to analysis in terms of deterministic models or to require a very complicated model. The demonstration that simple deterministic models can lead to complicated and irregular, or chaotic, behavior opened up the possibility of analyzing such data using deterministic models. Chaos is a phenomenon that has been found in many physical systems and has been confirmed both theoretically and experimentally. Chaos in a dynamical system is essentially characterized by the exponential divergence of initially adjacent trajectories as the system evolves in time. Manifestations of chaos involve a wide range of systems, such as mechanical, electrical, hydrodynamic, and biological processes, to name a few. Scientists and engineers have begun to appreciate the advantages of designing devices to exploit, rather than disregard, nonlinearity and chaos. Understanding chaos offers the possibility of control over some complex and elusive processes [14,15]. One important application where chaos theory has been shown to be beneficial is in the understanding and exploitation of fluid mixing [16]. In this case, a combination of chaos theory, fluid mechanics, and transport phenomena has produced a general framework that now can be used in a variety of practical situations [17].

IV. SIMULATION METHOD

We confine our study to non-Brownian suspensions in the regime of vanishingly small Reynolds number, $\mathrm{Re}_p \equiv \rho \dot{\gamma} a^2/\eta$. Here ρ and η are the density and viscosity, respectively, of the fluid, a is the radius of the suspended particles, and $\dot{\gamma}$ is the imposed shear rate.

For an accurate determination of the dynamics of suspended particles, and thereby the bulk properties of the suspension, the many-body hydrodynamic interactions between

particles must be computed correctly. This is accomplished by the Stokesian dynamics technique [18], which computes particle interactions as a sum of the far- and near-field hydrodynamic interactions in a consistent and efficient manner. Brady *et al.* [19] developed a method for simulating an infinite suspension of hydrodynamically interacting particles, by periodically replicating a finite number of particles throughout space. The lattice summation is carried out using the method of Ewald, to accelerate the convergence. For a detailed description of the above procedure, the reader is referred to Refs. [19–21].

Most studies that have employed Stokesian dynamics have only investigated unbounded uniform shear, ignoring the effect of boundaries. In realistic situations, flow is set either by the motion of the confining boundaries or driven by a pressure gradient, and the resulting dynamics can be quite different from that of unbounded systems. The impermeable walls alter the microstructure (i.e., the local arrangement of particles) near them, thereby altering the bulk properties.

Durlofsky *et al.* [20] were the first to incorporate the effect of plane boundaries in Stokesian dynamics simulations; they discretized the walls into patches, and accounted for interactions between the suspended spheres and the patches. However, they computed the interactions between spheres (or patches) far apart using a simplistic, mean-field, approach. Nott and Brady [1] computed the far-field interactions correctly, but approximated the wall as a planar lattice of spheres, creating a ''bumpy'' wall. To simulate plane walls more accurately, Singh and Nott [2] modified the procedure of Nott and Brady [1] by using the exact sphere-wall resistances while computing the near-field interactions, but used the bumpy-wall model for computing the far-field interactions. To simulate fully developed plane Couette flow, they introduced a layer of pure fluid adjacent to the layer of suspension in the master cell, which was then replicated periodically in the three directions. In this work, we follow exactly the procedure of Singh and Nott [2]; we briefly outline the simulation procedure below, and refer to their paper for a full description.

The master cell (see Fig. 1), containing a finite number of particles, is replicated periodically to achieve a suspension layer of infinite extent in the flow and vorticity directions. The velocities of the walls and the external forces on the suspended particles are specified. For computational convenience, we have performed monolayer simulations in which the spheres are restricted from translating in the z direction and the rotational movement of the spheres is allowed in the z direction only. Though this restriction will have an effect on the microstructure and therefore the bulk properties of the suspension, we expect that the essential physics of the problem is retained in a monolayer simulation [1,21].

The velocities of the suspended particles are given by

$$\boldsymbol{R}_{FU}^{ss}\times\boldsymbol{U}^{s}+\boldsymbol{R}_{FU}^{sw}\times\boldsymbol{U}^{w}=-\boldsymbol{F}^{s} \tag{1}$$

and the forces on the walls by

$$\boldsymbol{R}_{FU}^{ws}\times\boldsymbol{U}^{s}+\boldsymbol{R}_{FU}^{ww}\times\boldsymbol{U}^{w}=-\boldsymbol{F}^{w}. \tag{2}$$

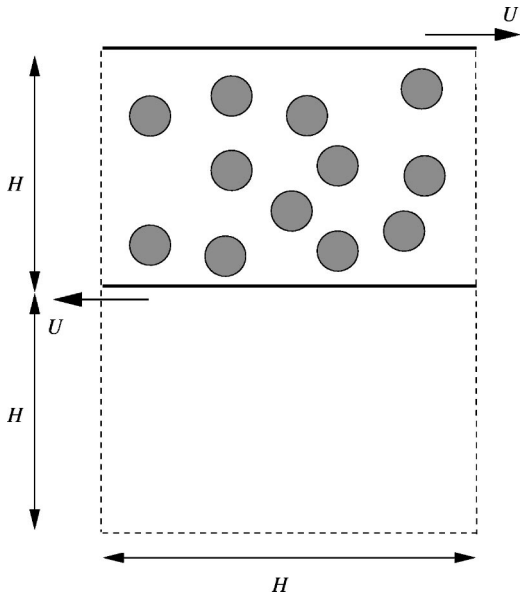

FIG. 1. A schematic representation of the master cell for our simulations. The layer of pure fluid allows us to periodically replicate the master cell and yet impose uniform shear in the suspension (see [2] for details).

Here, $\boldsymbol{U}^{s}$ is the vector of velocities of the suspended particles and $\boldsymbol{F}^{s}$ is the vector of (external) forces on them. Similarly, $\boldsymbol{U}^{w}$ and $\boldsymbol{F}^{w}$ are the velocities and forces, respectively, of the wall discretizations. The resistance $\boldsymbol{R}_{FU}$ depends only on the configuration, or the separation between particles, and the superscripts on it indicate the couplings between the spheres and walls (see Singh and Nott [2]). The shear stress σ_{yx} and the normal stress σ_{yy} are determined directly from the forces on the walls, but determination of the normal stress σ_{xx} is slightly more complicated (see [2] for details). Upon determining $\boldsymbol{U}^{s}$ for a given configuration, the particle positions are updated by integrating

$$\frac{d\boldsymbol{x}^{s}}{dt}=\boldsymbol{U}^{s}, \tag{3}$$

and the entire process of solving Eqs. (1)–(3) is repeated to continue the simulation.

While there is no external body force on the particles, we have imposed an interparticle repulsive interaction between them. Its main utility is in preventing the frequent particle overlaps which result from the finite time step in the simulation, but it also provides a qualitative model for nonhydrodynamic effects [20,22] when the interparticle separation is very small. The form of the repulsive force we have used is the same as in the simulations of [1],

$$\boldsymbol{F}_{\alpha\beta}=F_{0}\frac{\mu e^{-\mu\epsilon}}{1-e^{-\mu\epsilon}}\,\boldsymbol{e}_{\alpha\beta}, \tag{4}$$

where $\boldsymbol{F}_{\alpha\beta}$ is the force exerted by sphere β on sphere α. The parameters μ and F_{0} specify the range of the force and its

magnitude, respectively, ϵ is the separation between the surfaces of the spheres, and $\mathbf{e}_{\alpha\beta}$ is the unit vector connecting the sphere centers.

In the results that follow, all lengths have been scaled by the particle radius a, time by a/U (see Fig. 1), forces by $6\pi\eta Ua$ (η being the viscosity of the suspending fluid), and stresses by $\eta U/H$.

The only parameters in the problem are the Couette gap H (rendered nondimensional by the particle radius a), the area fraction of particles ϕ, and the parameters F_0 and μ, which determine the repulsive interaction. The number of suspended particles N_p is related to ϕ and H by the relation $N_p=\phi/(\pi H^2)$. We computed the stresses for a range of these parameters, and analyzed their time series. Most of our results were obtained with $H=18, F_0=10^{-4}$, and $\mu=100$, and particle area fraction in the range $0.05-0.6$. We have studied the effect of H by performing simulations for $H=14,18,30$ for $\phi=0.2$ and F_0 and μ remaining as above. To study the sensitivity of our results to the repulsive interaction, we have performed simulations for $\mu=10, 100$, and 1000, keeping $F_0\mu=0.01$ for $\phi=0.4$ and $H=18$.

V. NONLINEAR TIME-SERIES ANALYSIS

Figures 2(a) and 2(b) show that the shear and normal stresses in a suspension of spheres subjected to plane Couette flow exhibit persistent temporal fluctuations. A detailed analysis of these irregular fluctuations in the stress, using topological and dynamical methods, may reveal significant features about the dynamical system. The basic feature in the analysis using nonlinear dynamical methods is the characterization of the attractor, a bounded subset of the phase space to which the system behavior eventually converges as it evolves in time. This characterization is based on the reconstruction of the attractor of the system using delay reconstruction or other similar methods. A critical review in implementing different methods for the characterization of an attractor of dynamical systems and its implications are given in [23] and references therein.

Let $\boldsymbol{x}(t)$ represent the dynamics of a system, $\boldsymbol{x}$ being the properties that identify its state. In an experiment, we may be able to measure only a single scalar as a function of time $y(t)$. For instance, in a fluid flow experiment we may be able to measure the pressure as a function of time. Since the pressure depends only on the state of the system, we have a functional relation $y(t)=h(\boldsymbol{x}(t))$, where h is the measurement function relating y to $\boldsymbol{x}$. We now define the delay coordinate vector $(y(t),y(t+\tau),y(t+2\tau),\ldots,y(t+(m-1)\tau))$ with time delay τ, and propose that it is related to $\boldsymbol{x}(t)$ by

$$\begin{aligned}\Phi(\boldsymbol{x}(t))&=(y(t),y(t+\tau),\ldots,y(t+(m-1)\tau))\\&=(h(\boldsymbol{x}(t)),h(\boldsymbol{x}(t+\tau)),\ldots,h(\boldsymbol{x}(t+(m-1)\tau))).\end{aligned}\tag{5}$$

Takens [24] showed that for autonomous and purely deterministic systems [i.e., a system of differential equations $\partial\boldsymbol{\xi}/\partial t=f(\boldsymbol{\xi}(\mathbf{t}))$ in which f is not explicitly a function of t], the delay reconstruction map Φ, a bicontinuous differentiable function (diffeomorphism) which maps the state $\boldsymbol{x}$ into an m-dimensional delay vector, is an embedding when $m\geqslant 2n+1$, where n is the dimension of the phase space in which the attractor of the dynamical system evolves. [We say that $\Phi:\boldsymbol{X}\rightarrow\boldsymbol{Y}$ is an embedding of one compact space $\boldsymbol{X}$ into another $\boldsymbol{Y}$, if there is a one-to-one correspondence between $\boldsymbol{X}$ and $\Phi(\boldsymbol{X})$ with Φ and Φ^{-1} continuous, such that it preserves the differentiable structure [25] of the attractor including such quantities as Lyapunov exponents, dimension estimates, etc.] This theorem, called Takens' embedding theorem, asserts that if the attractor dimension is n, then for a complete understanding of the attractor, $2n+1$ dimensions in the embedded space are sufficient. Further generalizations [26,27] assert that any embedding dimension larger than the box counting attractor dimension (see Sec. V B) is sufficient, and in most cases the smallest integer greater than the correlation dimension (see Sec. V B) is sufficient for a complete characterization of the attractor [28]. Hence most of the significant characteristics, dynamical and geometrical, of the original system are carried over to the reconstructed phase space. Mathematically speaking, the characteristics of the original phase space are topologically and metrically equivalent to its mirror dynamical flow in the reconstructed phase space, i.e., the orbits of the original phase space are transformed into

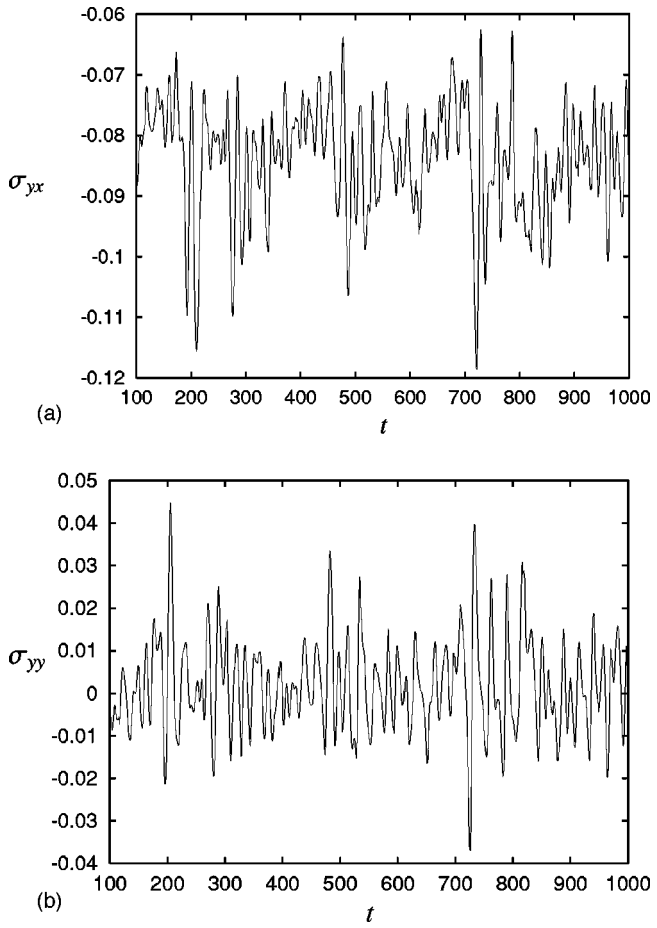

FIG. 2. Typical examples of the time series of the dimensionless shear (a) and normal (b) stresses against dimensionless time, shown here for $H=18$ and $\phi=0.2$.

orbits in the reconstructed phase space in such a way that their sense of orientation is preserved. Further, topological properties such as the number of significant eigenvalues, and dynamical and metrical properties such as Lyapunov exponents and different types of dimension measures (correlation dimension, Lyapunov dimension, box counting dimension, information dimension, etc.), are preserved [25]. In view of embedding theory, we can estimate the various dimensions and Lyapunov exponents, and perform reasonable predictions of future events based on this mapping.

A. Choosing the time delay ς

A direct application of the embedding theorem in real situations is impractical as it is valid only for an infinitely long and noise-free time series of a dynamical system. In principle, there is no restriction on the choice of the time delay. In practice, however, proper choice of both time delay and embedding dimension are of great significance and the information contained in a time-delay representation of real data is greatly influenced by the choice of these embedding parameters. Noise is usually of frequencies higher than those of the inherent dynamics of the system, and therefore imposes a lower bound on the time delay; using a time delay smaller than the largest significant noise time period will result in artificially high dimension. Even in the absence of noise, choosing too small a time delay will illustrate only the temporal correlation in the data, rather than its chaotic dynamics. Using too large a time delay runs the risk of missing genuine variations at smaller time scales. Thus, the optimal time delay is one for which the characteristics of the dynamics observed in the embedded space are not due to noise and temporal correlations of points, on the one hand, but the inherent dynamics of the system are not left out on the other. This can be quantified by using the autocorrelation function

$$\mathcal{A}(\varsigma)=\sum_n (x_n-\overline{x})(x_{n+\varsigma}-\overline{x}), \tag{6}$$

which is a normalized measure of the linear correlation among successive values of a time series $\{x_n\}_{n=1}^N$. Above, $\overline{x}$ is the temporal mean of the time trace $\overline{x}=(1/N)\Sigma_{n=1}^N x_n$. The decay of the autocorrelation with ς is a direct way to determine the decorrelation lag time (the time needed for the system to ''forget'' its initial conditions). The optimal time delay can be taken as the value of ς at which the autocorrelation function attains its first zero [29], or its first local minimum.

The time-delayed average mutual information $\mathcal{I}$ is also a tool to determine a reasonable delay. A distinguishing feature of $\mathcal{I}$ over the autocorrelation function is that it takes into account the nonlinear correlations in the data; it is given by

$$\mathcal{I}=-\sum_{ij} p_{ij}(\varsigma)\ln\frac{p_{ij}(\varsigma)}{p_i p_j}, \tag{7}$$

where p_i is the probability that one data point (observation) falls in the ith interval for some partition on the real numbers and $p_{ij}(\varsigma)$ is the joint probability that an observation falls into the ith interval and the observation time ς later falls into the jth interval. Here too the optimal delay is that corresponding to the first minimum or zero of $\mathcal{I}$. Another method to find a proper time lag is the space-time separation plot [30]. This procedure estimates the time lag for the system to free itself from the temporal correlations of points in phase space [6].

B. Choosing the embedding dimension m

The next crucial problem in nonlinear time-series analysis is to fix the number of independent coordinates required to reconstruct the attractor governing the dynamics of the system. The usual procedure is the following: a value of m is assumed and the data embedded in m-dimensional space. The volume of the resulting set is then determined by counting the number of m-dimensional cubes of size ϵ needed to enclose the set. The box counting dimension of the attractor is then given by

$$D_0=\lim_{\epsilon\to 0}\frac{\ln N(\epsilon)}{\ln(1/\epsilon)}. \tag{8}$$

In practice, $N(\epsilon)$ is determined for various embedding dimensions starting from unity, over a range of ϵ. If the plot of $\ln N(\epsilon)/\ln(1/\epsilon)$ against ϵ shows a plateau at approximately the same value for a sufficiently large range of ϵ for all embedding dimensions greater than a critical value m_c, a good approximation to the box counting dimension of the attractor is m_c. In computing the box counting dimension of an attractor, equal importance is given to all the cubes that enclose the data in phase space. However, for attractors having a fractional dimension, certain regions in phase space are visited more frequently by the trajectory and hence greater weightage should be given to cubes in that region. Grassberger [31], Grassberger and Procaccia [32], and others introduced the generalized dimension D_q which depends continuously on q as

$$D_q=\frac{1}{1-q}\lim_{\epsilon\to 0}\frac{\ln I(q,\epsilon)}{\ln(1/\epsilon)}, \tag{9}$$

where

$$I(q,\epsilon)=\sum_{i=1}^{N(\epsilon)} \mu_i^q, \tag{10}$$

where μ_i is the natural measure of cube i and the sum is taken for all the $N(\epsilon)$ cubes of size ϵ needed to enclose the attractor. Here the natural measure of cube i is given by

$$\mu_i=\lim_{T\to\infty}\frac{\eta(i,\boldsymbol{x}_0,T)}{T}, \tag{11}$$

where $\eta(i,\boldsymbol{x}_0,T)$ is the amount of time the orbit originating from a typical point $\boldsymbol{x}_0$ spends in the cube i in the time interval $0\leqslant t\leqslant T$ [33]. Of all the D_q dimensions, the correlation dimension D_2 is easiest to compute from a time series. Further simplification of D_2 from the above expression gives

$$D_2 = \lim_{r \to 0} \frac{\ln C_2(r)}{\ln r}, \tag{12}$$

where $C_2(r)$ is the correlation integral for radius r which obeys a scaling relation $C_2(r) \sim r^{D_2}$ in the limit $r \to 0$. [In general, for a self-similar structure, the correlation integral $C_q(\epsilon)$ of order q satisfies $C_q(\epsilon) \sim \epsilon^{(q-1)D_q}$ as $\epsilon \to 0$.] The correlation integral depends on the embedding dimension m of the reconstructed phase space as

$$C_2(r,m) = \frac{2}{N(N-1)} \sum_{i=1}^{N} \sum_{j=i+1}^{N} \Theta(r - \|\boldsymbol{x}(i) - \boldsymbol{x}(j)\|), \tag{13}$$

where $\Theta(a) = 1$ if $a > 0, \Theta(a) = 0$ if $a \leqslant 0, \boldsymbol{x}(t)$ is the m-dimensional vector of time-delay coordinates, and N is the length of the time series. The scaling exponent d increases with m and saturates to a final value D_2 for sufficiently large embedding dimension m_c [25]. In general, it is difficult to find a plateau region for a given value of m. Theoretically, D_2 has to be determined as the radius of the hypersphere r tends to 0 and m large. But in calculation small values of r are blurred by noise and limitations on the accuracy of the data and large values of m are not considered due to practical limitations. Practically, one finds a range (r_L, r_U) of r over which $\ln C_2(r,m)/\ln r$ gives an approximate plateau region with some tolerance $\pm \Delta m$.

For nonstochastic signals, the correlation dimension estimate is unaffected by small variations in the time delay. On the other hand, signals dominated by white noise will show statistically significant changes in the correlation dimension for different embedding dimensions, rarely converging to a fixed estimate of the correlation dimension as m increases (never converging for pure white noise), and small changes in time delay will affect the correlation dimension estimate significantly. In most cases, m_c is the smallest integer larger than D_2 [28]. When the exponent d of the correlation integral for various embedding dimensions reveals a plateau at low values of r and the plateau converges for increasing m, there is strong evidence for a low dimensionality of the underlying dynamics of the system. Usually, the correlation dimension from a time series is compared with other dimension estimates to ensure its veracity. In most cases it gives a good approximation to the number of equations required to model the system. Further, an accurate measurement of correlation dimension will reveal the possibility of a strange attractor if D_2 is not an integer.

Another technique for finding the minimum number of independent variables to describe the dynamics of the system is the false-nearest-neighbor (FNN) method [34,35]. The basic idea behind the method is that if an embedding dimension less than the actual dimension of the attractor is chosen, it will not unfold the true geometry of the attractor and there will be self-intersections leading to false neighbors. For example, if a sphere is embedded in two dimensions, the resulting structure will be a circular disk, and diametrically opposite points on the sphere (in the direction of projection) will become false neighbors. To determine the sufficient number of time-delay coordinates, one looks for the nearest neighbor $\boldsymbol{x}_d(j)$ in d-dimensional embedded space of each vector $\boldsymbol{x}_d(i)$, with respect to any metric. The distance $r_d(i,j)$ between the vectors in d-dimensional embedded space is then compared with the distance $r_{d+1}(i,j)$ if the data were embedded in $(d+1)$ dimensions. For instance, if the $\mathcal{L}_2$ metric is used, $r_{d+1}(i,j)$ can be written in terms of $r_d(i,j)$ as

$$r_{d+1}^2(i,j) = r_d^2(i,j) + [x(i + d\tau) - x(j + d\tau)]^2. \tag{14}$$

If $r_{d+1}(i,j)/r_d(i,j) \geqslant 1, \boldsymbol{x}_d(j)$ is a false neighbor of $\boldsymbol{x}_d(i)$; the cutoff value of the ratio in our calculations, above which the point is taken to be a false neighbor, is 10. If only a small fraction of the neighbors are false, d can be considered to be an embedding dimension for the dynamics of the attractor.

Use of both the above methods of finding the dimension of an attractor together leads to a good estimate of the actual dimension of the attractor, but neither of them can replace the other. Along with these methods, we used the principal component analysis to find the number of principal components (or significant eigenvalues) contributing to the dynamics of the system. We do not describe the procedure here, but refer the reader to Broomhead and King [36] for details. This method gives an upper bound to the number of independent coordinates required to reconstruct the attractor of the dynamical system. We also used some standard tools for the estimation of invariants of the dynamical system which we explain at the appropriate places below.

VI. RESULTS AND DISCUSSION

We restrict our attention to neutrally buoyant suspensions, where the densities of the suspended particles and the fluid are equal. The initial configuration of the suspended spheres was generated by first arranging the particles in a regular array and then applying small random displacements until a uniform distribution is reached. The system is allowed to evolve for about 5000 dimensionless time units and the velocity and stress fields are then recorded over the subsequent 95 000 time units. We used the softwares Chaos Data Analyzer Professional Version 2.1 of the Academic Software Library of the American Physical Society, the TISEAN Package [7], and visual recurrence analysis [37] for performing the tests on the time series.

A frequency decomposition of the shear stress shows a broadband spectrum (Fig. 3), which is characteristic of both deterministic chaos and a linear stochastic process [38,39]. The power spectrum shows an exponential decay with frequency, which again is common to deterministic chaos and linear autocorrelated noise. Therefore, a complete characterization of this behavior must be investigated by methods that can distinguish between deterministic chaos and linear autocorrelated noise (or a stochastic process). In this paper we use both the surrogate data analysis method and the visual recurrence analysis method, which are described below, to differentiate linear autocorrelated noise (or a stochastic process) from deterministic chaos.

The autocorrelation function of the shear stress time series converges to a local minimum at a time lag of roughly 17

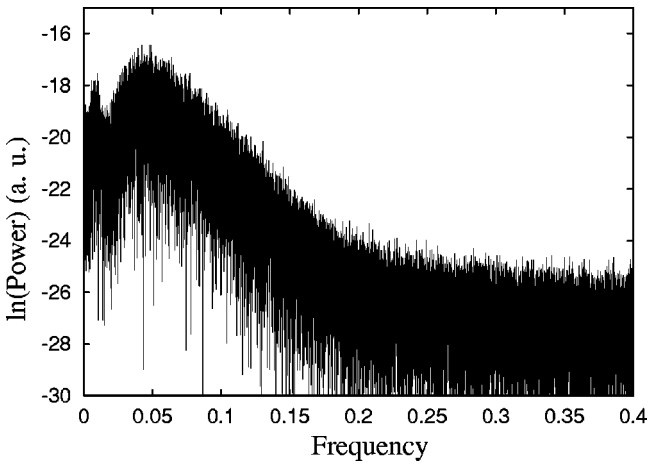

FIG. 3. Power spectral density of the normal stress σ_{yy} vs frequency (made dimensionless by scaling with the shear rate U/H) for $H=18$ and $\phi=0.2$. Exponential decay of the power with frequency is clearly seen, which is characteristic of both chaotic and linear stochastic signals.

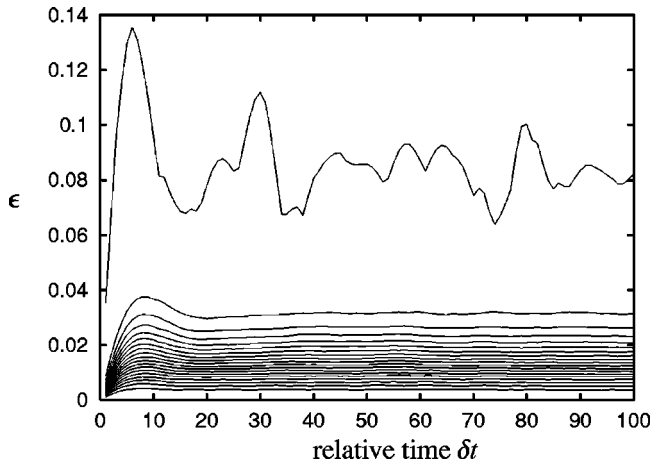

FIG. 4. Space-time separation plot of the normal stress σ_{yy} for $H=18$ and $\phi=0.2$. The lines are contours of probability densities 1/20, 2/20, 3/20, etc. (increasing in upward direction), for the normal stress at dimensionless time $t=t_0+\delta t$, with ϵ being different from that at $t=t_0$, averaged over all t_0.

time steps (a time step is equal to one dimensionless time unit). The average mutual information plot also shows roughly the same time delay. Along with these methods we used the space-time separation plot [30] to determine an optimal time delay. The importance of this method lies in excluding temporal correlations of points in phase space. That is, pairs of points which are measured within a short time span tend to be close in phase space and this will adversely affect the computation of the correlation integral. We use the correlation integral to compute the effective dimension of the underlying dynamics which is in no way related to the closeness of points in phase space due to temporal correlation. The idea in a space-time separation plot is that in the presence of temporal correlations the probability that a given pair of points has a distance smaller than ϵ does not only depend on ϵ but also on the time that has elapsed between the two measurements. This interdependence can be detected by plotting the number of pairs of points as a function of two variables, namely the time separation Δt and the spatial distance ϵ. In Fig. 4, contour lines are shown at the spatial distance ϵ where for a given temporal separation Δt, a fraction of 1/20,2/20, . . . of pairs are found. We observe a saturation of these contour lines above $\Delta t=17$. Hence this value can be regarded as a fair estimate of the decorrelation time which will exclude the influence of successive points due to temporal correlations.

The estimation of certain invariants, viz., correlation dimension, Lyapunov exponents, etc., requires a proper choice of Theiler's window ω [40], which provides guidelines for proper sampling of points from a time series of data. Theiler [40] suggested that all pairs of points whose time indices differ by less than ω may be ignored, where ω is approximately equal to the product of time lag and embedding dimension. For the computation of the correlation dimension, for instance, this requires the lower limit of j in Eq. (13) to be changed to $i+\omega$, and the factor multiplying the summation to be replaced by $(2/N)(N-\omega)$. Using the above information as a basis, we take Theiler's window as 100 for the estimation of certain invariant characteristics of the time series.

A. Low dimensionality of the attractor

In nonlinear time-series analysis, we are interested in characterizing the underlying attractor, a bounded limit set for typical initial conditions in some region of the phase space of the dynamical system. One of the parameters that characterizes an attractor is its dimension, which can be regarded as a measure of the amount of information necessary to specify the position of a point on the attractor within a given accuracy. For an accurate estimation of the attractor dimension, we the use principal component analysis, the false-nearest-neighbor method, and the Grassberger-Procaccia algorithm.

We performed a principal component analysis (see Sec. V B) on the normal and shear stresses for different particle area fractions. In this analysis, the dimension of the covariance matrix (see [36]) was chosen to be large enough that the significant eigenvalues did not vary much with the dimension. We get five significant eigenvalues (i.e., positive and greater than the noise floor) for $\phi=0.2$, between five and seven values for $0.2<\phi<0.5$, and above seven significant eigenvalues for $\phi>0.5$. This is illustrated in Fig. 5, which shows the eigenvalues obtained from a principal component analysis of the shear stress time series for three values of ϕ. As the number of significant eigenvalues is an upper bound for the dimension of the attractor [41,6], this is an indication that the number of independent coordinates required to capture the characteristics of the system increases with ϕ.

The false-nearest-neighbor method, described in Sec. V B, shows that the behavior of the attractor can be described by four or five independent coordinates as fractions of the false neighbors becomes very small at an embedding dimension of 5 (Fig. 6) when $\phi<0.4$. An estimate of the correlation dimension strengthens this conclusion. For an accurate estimation of the correlation dimension, we used the

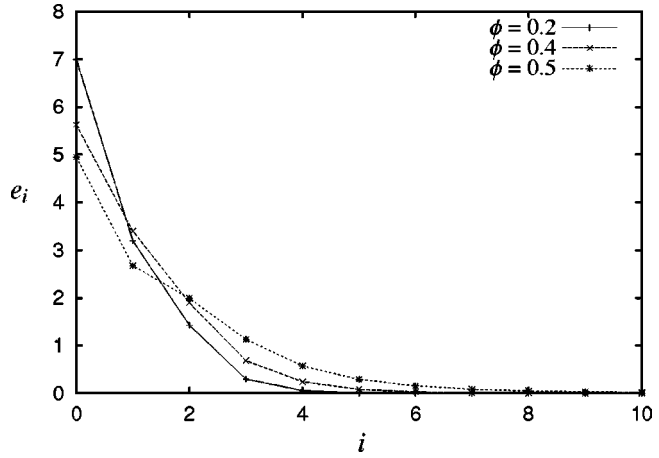

FIG. 5. The eigenvalues e_i in decreasing order of magnitude for the shear stress σ_{yx} for $H=18$.

Grassberger-Procaccia algorithm [32]. We took 95 000 data points of the time series of the normal and shear stresses, after deleting the initial transients, and computed the correlation integral for embedding dimensions ranging from 1 to 25 with a time delay $\tau=17$. The plot in Fig. 7 shows that the curves for high embedding dimensions converge in the range $0.27<r<0.37$, where $\ln C_2(r,m)/\ln r$ is approximately constant, indicating the existence of a low-dimensional attractor. However, the presence of local peaks in this region indicates the absence of clear correlation, and hence this method is not definitive in showing low dimensionality. We note, however, that this figure is typical of many in the literature. Moreover, the principal component analysis, the false-nearest-neighbor method, the nonlinear prediction method (discussed below), and the presence of structure in the three-dimensional phase-space plot all give strong indications of low dimensionality. In all the cases we obtained a fractional correlation dimension, indicating the existence of a low-dimensional strange attractor. The attractor dimension determined from the ''plateau'' region in Fig. 7 yields a correlation dimension between 2 and 4. Table I shows the correlation dimension of the normal and shear stresses for area fractions ϕ between 0.2 and 0.6. We observe that for any given particle concentration the correlation dimension estimates from the normal and shear stress time series are quite close. It is also apparent that the correlation dimension increases with area fraction.

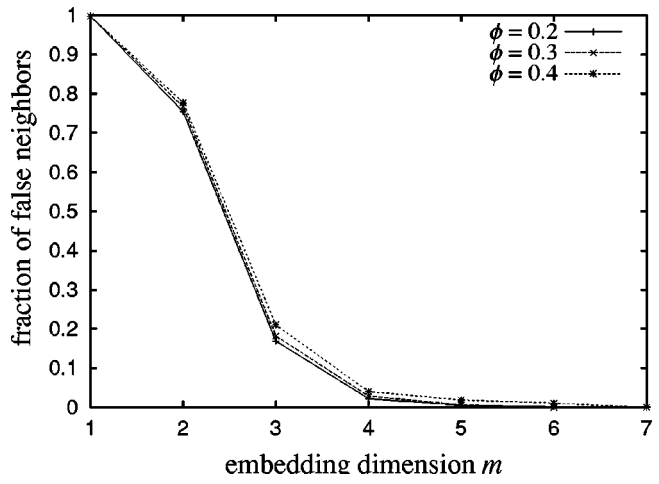

FIG. 6. Fraction of false nearest neighbors as a function of the embedding dimension m for the σ_{yx} time series, for $H=18$.

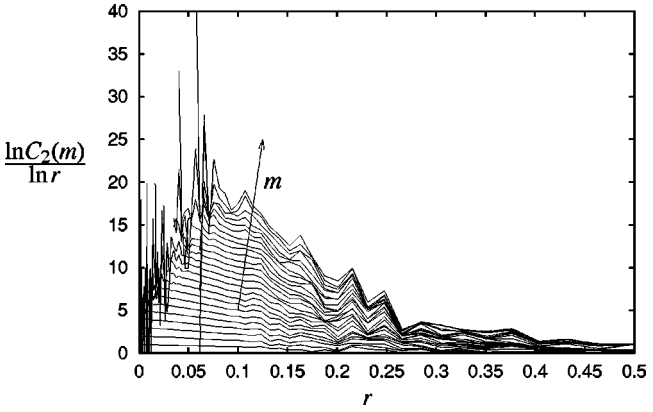

FIG. 7. A ''plateau'' of $\ln C_2(r,m)/\ln r$ in the region $0.27<r<0.37$ giving an approximate value of correlation dimension D_2. The correlation integral $C_2(r,m)$ was determined for the time series of the normal stress σ_{xx}, for $H=18$ and $\phi=0.2$. Though this test is not definitive, as there are local peaks within the plateau region, the plateau converges for higher embedding dimension, indicating evidence for low dimensionality of the attractor.

In high-dimensional systems, the prediction of succeeding data points is a robust method for estimating the dimension of the underlying attractor. The embedding dimension at which the prediction error is a minimum is a good estimate of the dimension of the attractor. We used the locally constant predictor method (see Sec. VII) for predicting *one-step ahead* the successive fluctuations of the stresses. We used 13 000 data points in the time trace of the shear or normal stress to determine the structure of the underlying attractor, and predicted the evolution for 35 succeeding dimensionless time steps. We then computed the normalized mean-square error (NMSE) of prediction. We observed that for an area fraction less than 0.4, the NMSE is minimum when the embedding dimension is 3 or 4. All these tests put together indicate strong evidence for the low dimensionality of the underlying attractor.

To study the influence of the Couette gap H on the invariant properties, we analyzed the time series of the stress com-

TABLE I. Correlation dimension D_2 determined from the time series of σ_{yy} and σ_{yx}, for $H=18$ and a range of the area fraction ϕ. Note that the estimates of D_2 from the two stress components are quite close, and are much smaller than the number of degrees of freedom $2N_p$. Also note the increase in D_2 with particle concentration ϕ.

		D_2	
ϕ	N_p	σ_{yx}	σ_{yy}
0.2	21	3.2	3.4
0.4	42	4.1	4.2
0.5	48	4.8	4.3
0.6	63	5.5	5.5

TABLE II. Correlation dimension determined from time series of σ_{yy} and σ_{yx} for different Couette gaps, $H=14$,18, and 30 for $\phi=0.2$. There is a slight decreasing trend in D_2 with increasing H.

		D_2	
H	N_p	σ_{yx}	σ_{yy}
14	13	3.7	3.8
18	21	3.2	3.4
30	57	3.0	3.0

ponents for $H=14$,18, and 30. Table II gives the correlation dimension for an area fraction $\phi=0.2$. We observe a slight decrease in the correlation dimension as the Couette gap increases. This is in agreement with the trend of the principal components (eigenvalues) for the above data, shown in Fig. 8. We also determined the correlation dimension for different values of μ, the range of the repulsive interparticle interaction (keeping $F_0\mu=0.01$) for a Couette gap of $H=18$, and a particle concentration $\phi=0.4$. These results are tabulated in Table III; it is apparent that there is no significant variation in the correlation dimension with μ.

The second columns in Tables I and II give the number of particles N_p in the simulations; the number of degrees of freedom is $2N_p$, as two Cartesian coordinates determine the position, and hence all other properties, for each particle. Comparing N_p and D_2, it is clear that the apparent dimension of the system is always far smaller than the number of degrees of freedom.

B. Deterministic nature of the system

A finite length time series with a broadband power spectrum may be a realization of a stochastic process governed by an autoregressive moving average model or of a low-dimensional deterministic chaotic process [42]. Further, some geometrical or dynamical characteristics (low correlation dimension or positive Lyapunov exponent, etc.) of the low-dimensional chaotic dynamics can be observed from

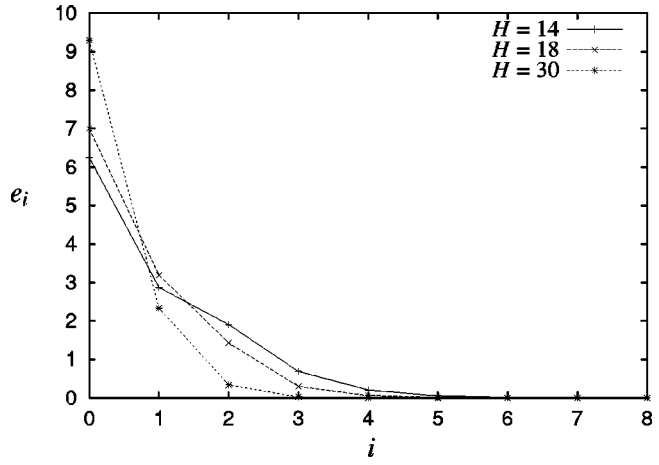

FIG. 8. The eigenvalues e_i in decreasing order of magnitude for the shear stress σ_{yx}, for Couette gaps $H=14$, 18, and 30 at $\phi=0.2$.

TABLE III. Correlation dimension determined from time series of σ_{yy} and σ_{yx} for different ranges of the interparticle repulsive force, $\mu=10$, 100, and 1000 (with $F_0\mu=0.01$). The data are for $H=18$ and $\phi=0.4$, with the number of particles $N_p=43$. Note that D_2 is relatively insensitive to changes in μ.

	D_2	
μ	σ_{yx}	σ_{yy}
10	4.3	4.2
100	4.1	4.2
1000	4.2	4.1

particular linear stochastic dynamics. Hence, the analysis of a time series has to distinguish between linear stochastic and deterministic dynamics. We used both surrogate data analysis and the visual recurrence analysis (VRA) method [37] to make this distinction. According to surrogate data analysis theory, the geometrical and dynamical characteristics of a time series must be compared with those of stochastic signals which have the same power spectrum and amplitude distribution as the original data [3]. One surrogate of a time series which tests for linear stochastic processes is obtained by randomizing the phases of the Fourier coefficients of the time series. One takes an ensemble of surrogates of the time series to compare with the original time series. In order to distinguish the nonlinear deterministic process from a linear stochastic process, we use a discriminating static Q defined by

$$Q=\frac{\mu_{\rm obs}-\mu_{\rm sur}}{\sigma_{\rm sur}}, \tag{15}$$

where $\mu_{\rm obs}$ is a characteristic measured from the original time series, $\mu_{\rm sur}$ is the average value of the same characteristic measured from the ensemble of surrogates, and $\sigma_{\rm sur}$ is the standard deviation of the characteristic for the ensemble of surrogates. We computed the correlation dimension of ten sets of such phase-shuffled time series for the shear and normal stresses. We found that $10<Q<15$, i.e., the correlation dimension of the original time series differs by 10 to 15 standard deviations from the mean correlation dimension of the ensemble of surrogates, clearly indicating that the difference is statistically significant. We also used the VRA method to determine the presence of structure in the stress fluctuations. The importance of the recurrence plot, one of the tools available in the VRA, is that the presence of structure can be visualized by means of color graphics. Once the dynamical system is reconstructed by means of delay coordinates, the distance between all pairs of vectors $\boldsymbol{x}(i)$ and $\boldsymbol{x}(j)$ is computed and various color codes are assigned to different distances. In a two-dimensional recurrence plot, a color code at the (i,j) position specifies the distance between the vectors $\boldsymbol{x}(i)$ and $\boldsymbol{x}(j)$. For random signals, a uniform distribution of colors over the entire plane is obtained and for deterministic signals we obtain coherent structures in the recurrence plot. This method demonstrated the existence of a coherent structure in the stress fluctuations in the suspension [Fig. 9(a)]. We also computed the spatio-temporal entropy for the stress. This quantity compares the distribution of col-

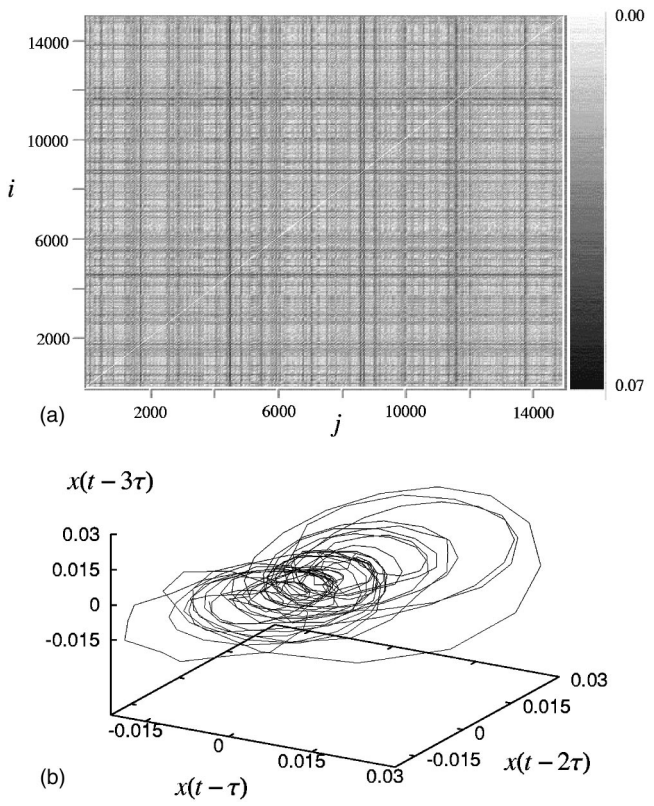

FIG. 9. (a) Recurrence plot for the dimensionless shear stress σ_{yx} for $H=18$ and $\phi=0.2$. The definite structure in the plot is apparent; data with white noise yield a uniform distribution of color. The axes labels *i* and *j* are index numbers of the data points in the time series. The color bar on the right indicates the distance-color mapping, with white representing zero distance and black representing the largest distance. (b) Phase-space plot of the dimensionless normal stress σ_{yy}, for $H=18, \phi=0.2$, and $\tau=17$.

ors over the entire recurrence plot with the distribution of colors over each diagonal line ($j=i+\text{const}$) of the recurrence plot. The higher the combined differences [43] between the global distribution and the distributions over the individual diagonal lines, the more structured the image is. In physical terms, this compares the distribution of distances between all pairs of vectors in the reconstructed state space with the distribution of distances between different orbits evolving in time (for details, see [44]). For random signals the value of spatio-temporal entropy will be close to 100% and for deterministic signals the value will be considerably less. The calculated values of the spatio-temporal entropy for the shear and normal stresses were nearly zero, showing perfect structure in the data. We observed definite structure in the phase-space plot of the stress components [Fig. 9(b)]. The predictability of the signal is also strong evidence for the deterministic nature of the system. From the above tests, we conclude that the fluctuations in the normal and shear stresses are due to a low-dimensional deterministic process.

C. Chaotic nature of the system

A striking behavior of some dynamical systems is their sensitive dependence on initial conditions, i.e., the divergence with time of trajectories from arbitrarily close initial conditions. An aperiodic bounded system having a sensitive dependence on initial conditions is termed a chaotic system. To determine the existence of such behavior in our system, we computed the stress for two slightly different initial distribution of particles (the position of a pair of particles differed slightly in the two initial configurations). Figure 10(a) shows the rapid divergence of the shear stress for the two initial configurations. The difference between the shear stresses of the two trajectories increases exponentially [Fig. 10(b)] for small *t*. Computing this exponential divergence of arbitrarily close trajectories over a time interval is of great significance in analyzing a time series obtained from a dynamical system. For a comprehensive characterization of the underlying attractor, we computed the maximum Lyapunov exponent (computation of the complete spectrum of Lyapunov exponents is tedious and requires a large amount of data), which measures the average rate of divergence or convergence of nearby orbits. The existence of a positive Lyapunov exponent is strong evidence for the chaotic nature of the system.

Several methods have been reported in the literature for efficient and accurate estimation of Lyapunov exponents, and we use the method developed by Kantz [45]. For computing the maximum Lyapunov exponent, we consider the representation of the time-series data as a trajectory in the embedding space. Then we construct a neighborhood $\mathcal{U}_n$ with radius r and center $\boldsymbol{x}_{n_0}$ in the embedded space. Let $\boldsymbol{x}_n$ be a very close return of the previously visited point $\boldsymbol{x}_{n_0}$; then $\Delta_0=\boldsymbol{x}_{n_0}-\boldsymbol{x}_n$ is a small perturbation. If one finds that its future $\Delta_t=\boldsymbol{x}_{n_0+t}-\boldsymbol{x}_{n+t}$ is given by $|\Delta_t|\approx\Delta_0 e^{\lambda t}$, then λ is the maximal Lyapunov exponent. Using the Kantz method [46,6], we compute

$$S(r,m,\Delta n) = \frac{1}{N}\sum_{n_0=1}^{N} \ln\left(\frac{1}{|\mathcal{U}(\boldsymbol{x}_{n_0})|} \sum_{\boldsymbol{x}_n \in \mathcal{U}(\boldsymbol{x}_{n_0})} \left| \boldsymbol{x}_{n_0+\Delta n} - \boldsymbol{x}_{n+\Delta n} \right| \right) \tag{16}$$

for a point $\boldsymbol{x}_{n_0}$ of the time series in the embedded space, where $\mathcal{U}(\boldsymbol{x}_{n_0})$ is the neighborhood of $\boldsymbol{x}_{n_O}$ with diameter r. If $S(r,m,\Delta n)$ increases linearly with Δn for small Δn, with identical slope for all dimensions m larger than some m_c and for a reasonable range of r, then the slope can be taken as an estimate of the maximal Lyapunov exponent λ. Here the effective expansion rate over a time span is averaged for a range of values of n_0. Figure 11 shows $S(r,m,\Delta n)$ increasing linearly with Δn, and the slope is roughly independent of the embedding dimension if it is greater than 4. The lines in Fig. 11 are for $m=4,5$, and for values of r in the range 5×10^{-5} to 10^{-3}. Our estimate of the maximum Lyapunov exponent from this figure is approximately 0.43.

The maximum Lyapunov exponents computed from the time traces of the normal and shear stresses, for a particle area fraction in the range 0.05–0.5, are tabulated in Table IV. The general trend of a rise in the maximum Lyapunov expo-

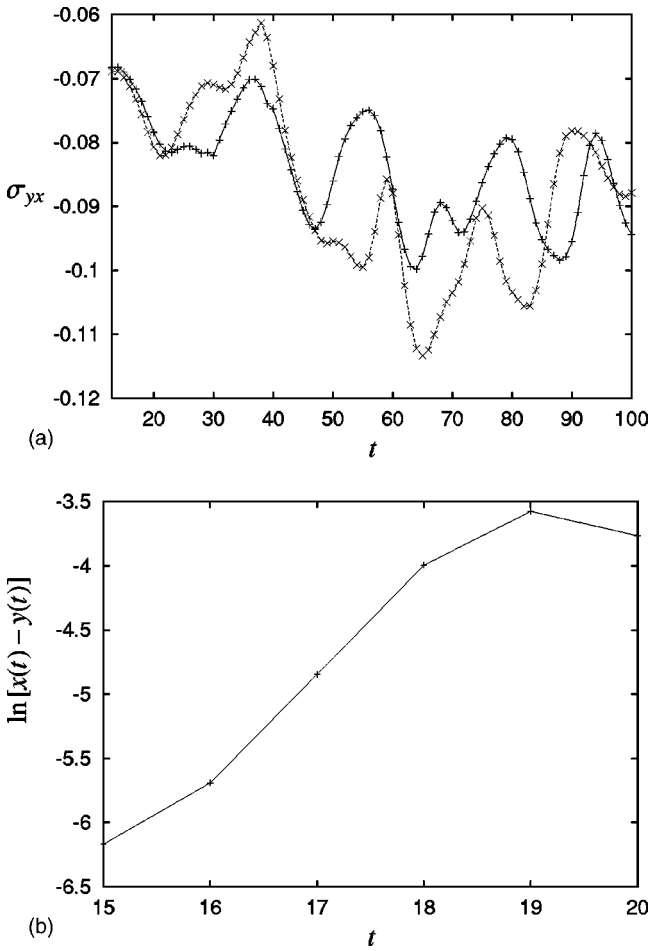

FIG. 10. Divergence of close trajectories $x(t)$ and $y(t)$ of the shear stress σ_{yx} for $H=18$ and $\phi=0.2$. (b) is the plot of the logarithm of the difference $x(t)-y(t)$ against dimensionless time t, showing clearly the exponential increase for small t in the difference between the stresses for the two trajectories in (a), indicating chaos.

nent with ϕ is apparent. This increase in the Lyapunov exponent is strong indication of many-particle interactions leading to chaotic behavior. We obtained numerical evidence for the presence of a chaotic attractor in the system even for the smallest area fraction of particles we considered. We also computed the entropy of the system, which indicates the chaotic nature of the system, defined in the following manner: If the system is embedded in m-dimensional space with delay τ, then the m dependence of the correlation integral $C_q(r,m)$ of order q for large m can be expressed [23,32,25] as

$$C_q(r,m)=\alpha(m)e^{-(q-1)h_q\tau m}r^{(q-1)D_q} \tag{17}$$

as $r\to 0$ and $m\to\infty$, where h_q is called the qth-order entropy. Computing the entropy for $q=2$ is the easiest, and it can be performed along with the computation of the correlation dimension D_2. Our calculations show that the entropy, which is always less than or equal to the sum of the positive Lyapunov exponents, is positive for all particle concentrations.

Further evidence of chaos is provided by the one-step-ahead and multistep-ahead predictions of successive fluctuations of the stresses (see Sec. VII). While the one-step-ahead successive prediction is quite accurate up to nearly 35 time steps in the future [Fig. 12(b)], the multistep-ahead prediction diverges from the actual time trace after 3–5 time units [Fig. 12(a)]. This apparent distinction between the two predictions is a clear indication of the sensitive dependence on initial conditions of nearby trajectories. Lastly, the power spectrum of the time series of the normal and shear stresses also shows exponential decay, indicating the chaotic nature of the signal (Fig. 3).

Given all the above evidence, we conclude that the attractor underlying the fluctuations in the stress has a fractional correlation dimension, and is a consequence of low-dimensional chaotic dynamics.

VII. PREDICTION OF SUCCESSIVE FLUCTUATIONS

As mentioned in Sec. III, an important feature of chaotic systems is their exponential sensitivity to initial conditions: the average error made when forecasting the outcome of a future measurement increases exponentially with time. The length of the period over which accurate short-term predictions of the successive fluctuations of the signal are possible is determined by the accuracy of the initial conditions and estimate of the Lyapunov exponent. We use local models to predict the one-step and multistep procedures. That is, instead of fitting one complex model with many coefficients to the entire data set, we fit many simple models (low-order polynomials) to small portions of the data set depending on the geometry of the local neighborhood of the dynamical system. The general procedure is the following: the last known state of the system, represented by a vector $\boldsymbol{x}=(x(n),x(n+\tau),\ldots,x(n+(m-1)\tau))$, is determined, where m is the embedding dimension and τ is the time delay. Then p close states (usually nearest neighbors of $\boldsymbol{x}$) of the system that have occurred in the past are found, by computing their distances from $\boldsymbol{x}$. The idea then is to fit a map which extrapolates $\boldsymbol{x}$ and its p nearest neighbors to determine the next values. Using this map, an approximate value of $x(n+1)$ can be obtained. We use both the one-step- and multistep-ahead prediction methods. In the one-step-ahead prediction, after each step in the future is predicted, the actual value is utilized for the next one-step prediction. In contrast, the multistep prediction is based only on the initial p states. The normalized mean-squared error (NMSE), referred to in Sec. VI A, is computed by comparing the mean-square error (between data and prediction) of the above method with the MSE of the unconditional mean predictor method (a trivial method which predicts the average of the observed values as the subsequent value). As stated in Sec. VI A, we observed that the NMSE is minimum when m is between 3 and 4 for ϕ less than 0.4, roughly 5 for ϕ between 0.4 and 0.5, and is above 5 for ϕ greater than 0.5.

From the time series of the stresses up to a given time t_0, we predicted their subsequent evolution (i.e., the multistep prediction) using the locally constant predictor (in VRA). A good prediction is possible only up to $t=t_0+3$, as shown in

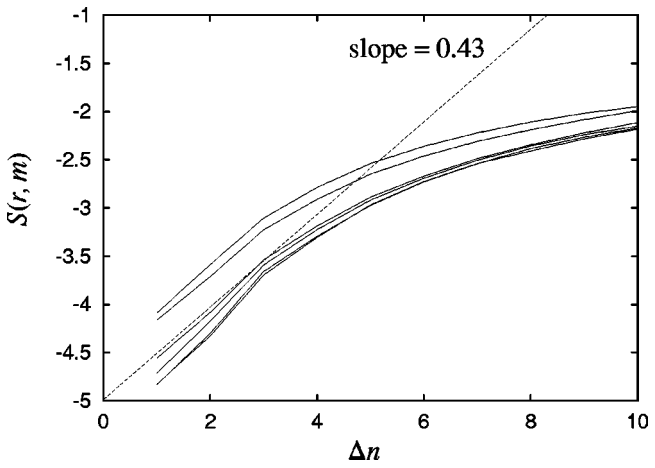

FIG. 11. The function $S(r,m,\Delta n)$ [see Eq. (16)] vs Δn for various embedding dimensions. The slope is approximately 0.43 (independent of m) for $m \geqslant 4$. Data are for the dimensionless normal stress σ_{yy} for $H=18$ and $\phi=0.2$.

Fig. 12(a). In contrast, the one-step-ahead prediction [37] of successive fluctuations of the stress is quite accurate for all time [Fig. 12(b)], indicating the deterministic nature of the system.

VIII. CROSS PREDICTION OF THE TIME SERIES

Cross prediction of one time series from the time series of another related variable was introduced recently by Abarbanel *et al.* [46]. This technique has potential application in situations where the measurement of one quantity is difficult or expensive, while the measurement of a related variable is easy or inexpensive. In such a case, simultaneous measurements of both variables need to be made for a baseline period, and then the easily measured variable can be used to predict the other. The cross prediction of a signal (response signal) $\boldsymbol{y}(t)$ from another signal (drive signal) $\boldsymbol{x}(t)$ implies the existence of a functional relation Ψ such that $\boldsymbol{y}(t) = \Psi(\boldsymbol{x}(t))$. One significance of this technique is that the prediction of one variable from another can be made without knowing the properties of Ψ. When the phase-space points of the driving and response systems are connected by such a functional relation Ψ, two nearby states in the phase space of the driving system correspond to two nearby states in the phase space of the response system. This property of a pair of such systems can be characterized by the mutual false-nearest-neighbors (MFNN) parameter [34]. For systems preserving this identity of neighbors in state space, the value of the parameter will be of the order of unity. We computed that the MFNN for the shear and normal stresses is close to unity. We used the nearest-neighbor method [7] to predict the normal stress from the shear stress time series, and the results for $\phi=0.4$ are shown in Fig. 13.

TABLE IV. The maximum Lyapunov exponent for the σ_{yy} and σ_{yx} time series, for $H=18$ and various particle concentrations ϕ. The Lyapunov exponent increases with ϕ, implying that the system is more chaotic when the particle concentration is increased.

	λ	
ϕ	σ_{yx}	σ_{yy}
0.05	0.25	0.22
0.1	0.33	0.18
0.2	0.42	0.34
0.3	0.42	0.35
0.4	0.43	0.42
0.5	0.49	0.45

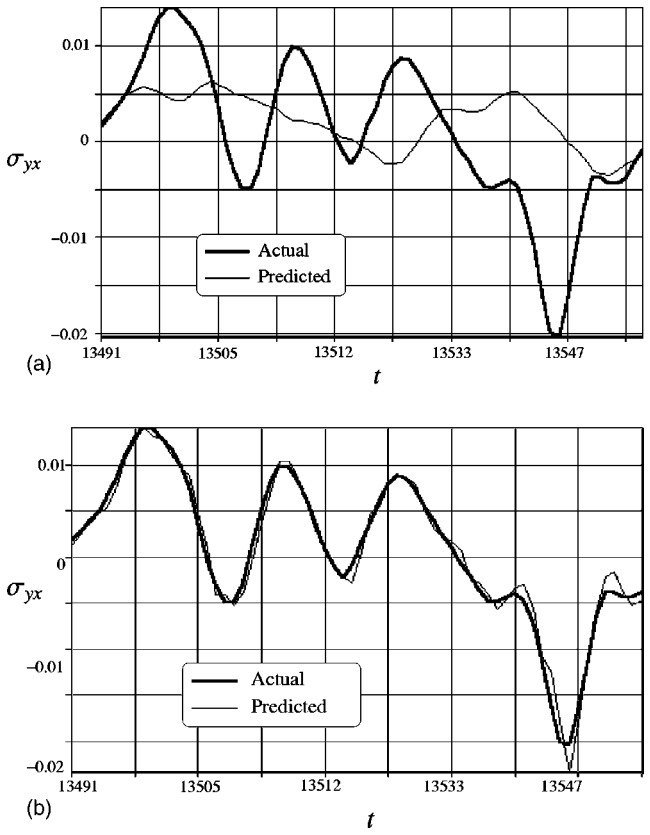

FIG. 12. Multistep (a) and one-step (b) predictions of the normal stress σ_{yy} for $H=18$ and $\phi=0.2$. Note the close agreement of the one-step prediction with the actual time trace.

IX. DISCUSSION

We have analyzed, using the tools of nonlinear dynamics and chaos theory, the fluctuations in the shear and normal stresses developed when a Stokesian suspension is subjected to simple shear flow. We have found numerical evidence for the existence of a low-dimensional chaotic attractor for particle area fraction ϕ in the range 0.05–0.6. We have used this information about the underlying structure in the fluctuations to make short-range predictions of the shear and normal stresses, and cross predictions of one component of the stress with knowledge of the other, with significant success. The rise in the correlation dimension and Lyapunov exponent with ϕ gives a clear indication of the influence of particle interactions on the chaotic response of the suspension. The existence of a low-dimensional chaotic attractor underlying

the fluctuations opens up the possibility of technological applications such as chaos control to temper the fluctuations.

For non-Brownian Stokesian suspensions, the instantaneous value of the stress is related to the instantaneous separation between particles, i.e., their configuration. The evolution of the n-particle configuration distribution function $f_n(\boldsymbol{r})$ is governed by the Smoluchowski equation [9], which reduces to a balance between accumulation and advection in the absence of Brownian motion,

$$\frac{\partial f_n}{\partial t} + \sum_{\alpha=1}^{n} \boldsymbol{\nabla}_\alpha \cdot (\boldsymbol{U}_\alpha f_n) = 0. \tag{18}$$

If the velocities $\boldsymbol{U}_\alpha$ are independent of f_n, it is clear that Eq. (18) yields a fixed point for f_n. This was the basic assumption of Batchelor and Green [8] and Brady and Morris [9]. However, for bounded shear flows of the kind considered in this work, and those one usually encounters in practice, the velocities are determined by the local viscosity of the suspension, which in turn is a function of the configuration. There is hence a coupling between Eq. (18) and the equations of motion of the suspension. The nonlinearity in the coupling in Eq. (18) allows the possibility of chaotic variation of the microstructure and therefore the stress, as is evident from our results.

For large samples and over long time scales, one intuitively expects that the evolution of the stress will be captured by a hydrodynamic description, an expectation that is in agreement with our observation of low dimensionality of the attractor. However, we must emphasize that this conclusion is not *a priori* obvious or evident: a suspension of macroscopic non-Brownian particles differs in a significant way from molecular fluid in that there is no inherent time scale (set by the temperature) in the system. The imposed shear rate, which is the time scale of macroscopic motion, is the only time scale in the problem and, therefore, there is no separation of time scales normally observed in molecular systems. In other words, the frequency of fluctuations in the stress scale is the imposed shear rate. Thus, low dimensionality is an interesting observation we make, rather than a foregone conclusion: even at the pair-interaction level, the position distribution function f_2 is a *field* which in the dynamical sense is an infinite-dimensional quantity. Our observation of low dimensionality of the stress fluctuations implies that only a few (between four and six) moments of the position distribution function contribute to the stress fluctuations. This appears to be an important and far-reaching result, as the task of connecting the microstructure to rheology is then much easier if we knew which of the moments of the former were the important ones and how to compute them.

A clear physical picture of the stress fluctuations can be obtained if we recognize that large fluctuations in the stress arise from the formation and breakage of clusters of many particles that sometimes span the distance between the bounding walls. In simple shear, for instance, clusters form in the compression quadrant where hydrodynamic forces squeeze particles together. The clusters are then rotated by the vorticity of the flow, and the particles in the cluster are pulled apart in the extension quadrant. The rate of formation and breakage of the clusters, which determines the frequency of the stress fluctuations, is determined by the local number density and mobility of clusters, and one therefore gets a range of frequencies, as shown in Fig. 3. We also note both the shear stress and the normal stress fluctuations have similar correlation dimensions and maximum Lyapunov exponent. Since both the shear stress and the normal stress are determined by an appropriate function of the microstructure, our results indicate that the dynamics of the microstructure is governed by a low-dimensional attractor having approximately the same correlation dimension and maximum Lyapunov exponent.

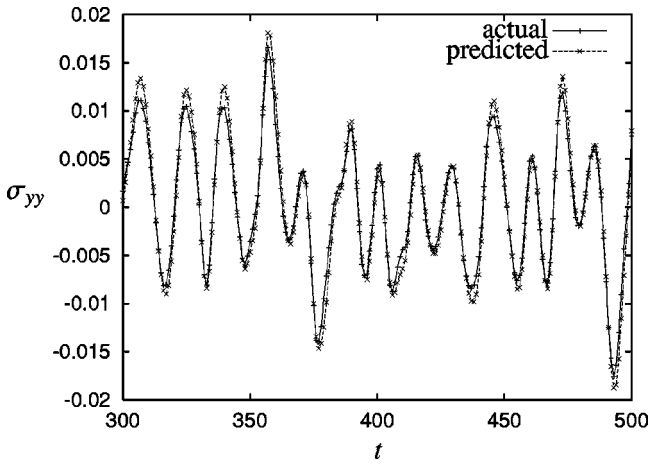

FIG. 13. Cross prediction of the normal stress σ_{yy} from the shear stress σ_{yx} for suspension with $\phi = 0.4$ and $H = 18$.

Comparing our simulations to a typical globally coupled map lattice, we note that the relative particle positions in our simulations correspond to the values attained by individual chaotic oscillators in a coupled map lattice, and the coupling between any two particles is a chaotic function of the difference in positions between any two particles. In a coupled map lattice sense, this would correspond to a globally coupled map lattice where the coupling is calculated by summing up a chaotic function of the difference in values at any instant between the oscillators (particles) taken pairwise. Our system thus represents a generalization of a typical globally and democratically coupled map lattice. This result may thus have significant implications for the theory of coupled map lattices.

ACKNOWLEDGMENTS

J.D. and T.R.R. thank Dr. G. Vijay Nair, Director, Regional Research laboratory (CSIR), Trivandrum, India for constant encouragement. Financial support from DST, New Delhi Grant Nos. III 5(90)/95-ET and SP/S2/E01/98 is acknowledged. We thank Al Farook Muhammed Ridha and Tito Paul for help with the figures. J.D. thanks CSIR, India for financial support.

[1] P.R. Nott and J.F. Brady, J. Fluid Mech. **275**, 157 (1994).
[2] A. Singh and P.R. Nott, J. Fluid Mech. **412**, 271 (2000).
[3] G.P. Pavlos, M.A. Athanasiu, D. Diamantidis, A.G. Rigas, and E.T. Sarris, Nonlinear Proc. Geophys. **6**, 51 (1999a).
[4] G.P. Pavlos, M.A. Athanasiu, D. Diamantidis, A.G. Rigas, and E.T. Sarris, Nonlinear Proc. Geophys. **6**, 79 (1999b).
[5] G.P. Pavlos, M.A. Athanasiu, D. Diamantidis, A.G. Rigas, and E.T. Sarris, Nonlinear Proc. Geophys. **6**, 99 (1999c).
[6] H. Kantz and T. Schreiber, *Nonlinear Time Series Analysis* (Cambridge University Press, Cambridge, England, 1997).
[7] R. Hegger, H. Kantz, and T. Schreiber, Chaos **9**, 413 (1999).
[8] G.K. Batcheler and J.T. Green, J. Fluid Mech. **56**, 375 (1972).
[9] J.F. Brady and J.F. Morris, J. Fluid Mech. **348**, 103 (1997).
[10] A. Einstein, Ann. Phys. (Leipzig) **19**, 298 (1906).
[11] F. A. Gadala-Maria, Ph. D. thesis, Standford University, 1979.
[12] I.E. Zarraga, D.A. Hill, and D.T. Leighton, J. Rheol. **44**, 185 (2000).
[13] A. Singh and P.R. Nott (unpublished).
[14] D.J. Christini, J.J. Collins, and P.S. Linsay, Phys. Rev. E **54**, 4824 (1996).
[15] M. Ciofini, R. Meucci, and F.T. Arecchi, Phys. Rev. E **52**, 94 (1995).
[16] D.A. Zumbrunnen, K.C. Miles, and Y.H. Liu, Composites, Part A **27A**, 377 (1996).
[17] J.M. Ottino, *The Kinematics of Mixing: Stretching, Chaos, and Transport* (Cambridge University Press, Cambridge, England, 1989).
[18] J.F. Brady and G. Bossis, Annu. Rev. Fluid Mech. **20**, 111 (1988).
[19] J.F. Brady, R.J. Phillips, J.C. Lester, and G. Bossis, J. Fluid Mech. **195**, 257 (1988).
[20] L. Durlofsky, J.F. Brady, and G. Bossis, J. Fluid Mech. **180**, 21 (1987).
[21] J.F. Brady and G. Bossis, J. Fluid Mech. **155**, 105 (1985).
[22] D.I. Dratler and W.R. Schowalter, J. Fluid Mech. **325**, 53 (1996).
[23] T. Schreiber, Phys. Rep. **308**, 1 (1999).
[24] F. Takens, *Detecting Strange Attractor in Turbulence*, Lecture Notes in Mathematics Vol. 898, edited by D.A. Rand and L.S. Young (Spinger, Berlin, 1981), pp. 366–381.
[25] E. Ott, Tim Sauer, and James A. Yorke, *Coping with Chaos* (Wiley, New York, 1994).
[26] T. Sauer and J. Yorke, Ergod. Theory Dyn. Syst. **17**, 941 (1997).
[27] T. Sauer and J. Yorke, Int. J. Bifurcation Chaos Appl. Sci. Eng. **3**, 737 (1993).
[28] M. Ding, C. Grebogi, E. Ott, T. Sauer, and J.A. York, Physica D **69**, 404 (1993).
[29] J. Holzfuss and G. Mayer-Kress, in *Dimensions and Entropies in Chaotic System. Quantification of Complex Behavior*, edited by G. Mayer-Kress, Springer Series in Synergetic Vol. 32 (Springer, Berlin, 1986), p. 114.
[30] A. Provenzale, L.A. Smith, R. Vio, and G. Murante, Physica D **58**, 31 (1992).
[31] P. Grassberger, Phys. Lett. **97A**, 227 (1983).
[32] P. Grassberger and I. Procaccia, Physica D **9**, 189 (1983).
[33] E. Ott *Chaos in Dynamical Systems* (Cambridge University Press, Cambridge, England, 1993).
[34] H.D.I. Abarbanel, *Analysis of Observed Chaotic Data* (Springer, Berlin, 1996).
[35] M.B. Kennel, R. Brown, and H.D.I. Abarbanel, Phys. Rev. A **45**, 3403 (1992).
[36] D. Broomhead and G.P. King, Physica D **20**, 217 (1986).
[37] E. Kononov, *Visual Recurrence Analysis*, Version 4.0, 1999 (email: eugenek@ix.netcom.com).
[38] H. Schuster, *Determininstic Chaos*, 2nd ed. (Physik-Verlag, Weinheim, Germany, 1988).
[39] A. Tsonis, *Chaos: From Theory to Application* (Plenum, New York, 1992).
[40] J. Theiler, J. Opt. Soc. Am. A **7**, 1055 (1995).
[41] A.M. Albano, J. Muench, C. Schwartz, A.I. Mees, and P.E. Rapp, Phys. Rev. A **38**, 3017 (1988).
[42] J.P. Eckmann and D. Ruelle, Rev. Mod. Phys. **57**, 617 (1985).
[43] J.A. Peacock, Mon. Not. R. Astron. Soc. **202**, 615 (1983).
[44] T.W. Carr and I.B. Schwartz, Physica D **115**, 321 (1998).
[45] H. Kantz, Phys. Lett. A **185**, 77 (1994).
[46] H.D.I. Abarbanel, T.W. Frison, and Lev Sh. Tsimring, IEEE Signal Process. Mag. 49 (1998).